2015 IEEE 54th Annual Conference on Decision and Control (CDC)
December 15-18, 2015. Osaka, Japan

# Modeling, observer design and robust control of the particle density profile in tokamak plasmas

T.C. Blanken, F. Felici, M.R. de Baar, W.P.M.H. Heemels and the TCV team[1]

*Abstract*— **A new approach to real-time estimation and feedback control of the particle density profile in tokamak plasmas is presented, based on ideas from Kalman filtering and $H_\infty$ robust control synthesis. Traditionally, the density profile is reconstructed in real-time by solving an inversion problem using a measurement from a single time instant. Such an approach is sensitive to sensor errors and does not account for the dynamical evolution and spatial continuity of the density. The observer-based approach we presented here includes the system dynamics, which is realized by careful modeling of the particle density behaviour using a 1D PDE with a nonlinear source term and two ODEs, which are discretized in space and time to yield a finite-dimensional nonlinear model. The influence of other plasma quantities and operational modes on the transport dynamics are included in the control-oriented model as time-varying parameters. An extended Kalman filter estimates the density, additive random-walk state disturbances as well as fringe jumps (a specific type of sensor error) from measurements, for which special measures are needed. Offline reconstruction using tokamak measurements show accurate estimation of the density profile and show the quality of fringe jump detection. Moreover, a robust state feedback controller with anti-windup is designed based on the model to track a reference signal for the average density, with the estimate obtained from the observer. Closed-loop simulations show that the controller is able to track representative reference signals, with the performance mostly limited by the nonnegativity constraint of the control input.**

## I. INTRODUCTION

The tokamak, a device for magnetic confinement of a hot plasma, has been a promising candidate for several decades to reach controlled thermonuclear energy production. Plasma confinement is realized by a combination of magnetic fields from external coils and induced current in the plasma. A key challenge in tokamak operations is maintaining stable plasma conditions, remaining within safety limits and accurate control of the plasma state.

Up to now, relatively little attention is paid to reconstruction and control of the spatial distribution of the particle density. However, as the density profile affects fusion power but also drives undesirable radiation and can trigger detrimental plasma instabilities, real-time safety monitoring and control of the particle density is of great importance for safe, reliable and high-performance operation of tokamaks.

Thomas Blanken and Marco de Baar are with FOM-institute DIFFER, Association EURATOM-FOM, PO Box 1207, 3430 BE Nieuwegein, The Netherlands. t.c.blanken@tue.nl

Thomas Blanken, Federico Felici, Marco de Baar and Maurice Heemels are with the Control Systems Technology group at the Department of Mechanical Engineering, Eindhoven University of Technology, PO box 513, 5600 MB Eindhoven, the Netherlands.

[1]École Polytechnique Fédérale de Lausanne (EPFL), Center de Recherches en Physique des Plasmas, CH-1015 Lausanne, Switzerland.

Existing feedback control systems for the density (e.g. [1], [2]) focus on tracking a reference signal for a single measurement channel of an interferometry system. Such interferometry systems, commonly installed on tokamaks, measure the line-integrated electron density along one or more laser chords intersecting the plasma at different locations [3]. Existing methods on real-time estimation the density profile work by minimizing a least-squares criterium on multiple interferometry measurements at one instant in time only. However the estimates suffer from spatial oscillations and are sensitive to sensor errors [1]. PID controllers tuned by hand provide satisfactory tracking performance, but have to be re-tuned for varying operating conditions of the tokamak.

In recent work on model-based control of the profiles of temperature and current [4], it has been assumed that the to-be-controlled quantities are known in real-time. This assumption is hard to realize in practice, since on many tokamaks the current density profile can not be reliably and accurately determined in real-time due to a lack of suitable measurements. Similarly, the density profile is not directly measured. There has been work on using model-based state observers for the current and temperature profiles [5], but this did not include estimation of the density profile.

For accurate real-time estimation and control, calculations have to be completed faster than the time scale on which the density changes. Existing high-fidelity models are often not suitable for this task. Indeed, transport in a tokamak plasma is modeled by the combination of a set of 1D PDEs for radial transport and a 2D elliptical PDEs for the plasma magnetic equilibrium (see [6], [7]). Physics-based models for the plasma particle transport (e.g. [8], [9]) and profile reconstruction algorithms for offline data analysis (e.g. ASTRA [7], CRONOS [10]), are not suited for use in a real-time observer/controller due to their high complexity and computational cost. On the other hand, compact multi-inventory (0D) models for density control have appeared [2], [11], but these did not consider the spatial distribution of the density.

Inspired by earlier work in [5], we propose in this paper to use a model-based state observer to provide better estimates of the density profile in real-time for the purpose of feedback control. We present a control-oriented nonlinear model for the spatial distribution of the plasma density with two additional particle inventories. Compared to existing multi inventory models [2], [11], we replace the plasma inventory by the spatial distribution of the plasma density. Moreover, we include the influence of plasma equilibrium, temperature, current and operational modes of the tokamak

on the transport dynamics as an exogeneous input parameter, thereby obtaining a nonlinear model suitable for real-time estimation of the density profile.

Based on this new control-oriented model, we design an extended Kalman filter (EKF) to estimate the density from interferometry measurements. Modeling errors are interpreted as additive disturbances on the density, to be estimated by the observer. We propose to detect a specific type of sensor errors, called fringe jumps [12], by inspection of the discrepancy between the measurements and the model-based predictions of the measured quantities. Fringe jumps originate from phase counting errors in the interferometer due to fast changes in the plasma density and appear as sudden offsets of an integer multiple of $2\pi$ in the output signals. Despite ongoing research on detection and correction of fringe jumps [1], [12], [13], [14], no definitive satisfactory solution has been found. Therefore we propose to include a fringe jump description and detector in the EKF.

Reliable real-time estimation of the density profile opens the way for high-performance feedback control. In this paper, we propose to use model-based $H_\infty$ robust control synthesis as an aid in designing controllers that are robust against modeling errors, disturbances and varying dynamics (accounted for as changes in the parameter). We design a state feedback controller to track a reference signal of the average density, based on the estimate obtained by the observer. We will illustrate the satisfactory behavior of the interconnection of observer and controller using simulations.

The remainder of this paper is structured as follows. A control-oriented model of the relevant input-output behaviour is introduced in Section II. The design of the state observer, the detection of fringe jumps and the offline estimation results on experimental data are discussed in Section III. The feedback control design and simulations of the closed-loop system including observer and controller are discussed in Section IV. Finally, concluding remarks and an outlook to future research are given in Section V.

## II. Model of the particle transport

In this section, we present a generic model of the particle transport in tokamaks for the purpose of observer and controller design. This model has the flexibility to adapt to multiple tokamaks, diagnostics and actuators and encompasses the time evolution of the electron density $n_e(\rho,t)$, the inventories of the neutral vacuum $N_v(t)$ and the wall $N_w(t)$ to the available actuators, where $\rho$ denotes the spatial coordinate on which density changes and $t$ denotes time. See Figure 1 for a schematic representation of the plasma cross section. We discretize the PDE in space and then discretize the resulting set of ODEs in time. The relation between plasma density and measured quantities is then added to form a state-space representation of the system.

We choose control-relevant models to prevent a high numerical complexity and a large amount of unknown physical coefficients. We account for the influence of edge electron temperature $T_{e,b} = T_e|_{\rho=1}$, electrical current $I_p$, 2D equilibrium $\rho(r,Z)$ and distinct operational regimes (limited or diverted plasma $c_{ld} \in \{0,1\}$, low or high confinement mode $c_{lh} \in \{0,1\}$) on the transport dynamics with a time-varying exogeneous input parameter. We assume that estimates of these parameter values are available through real-time equilibrium reconstruction and measurements.

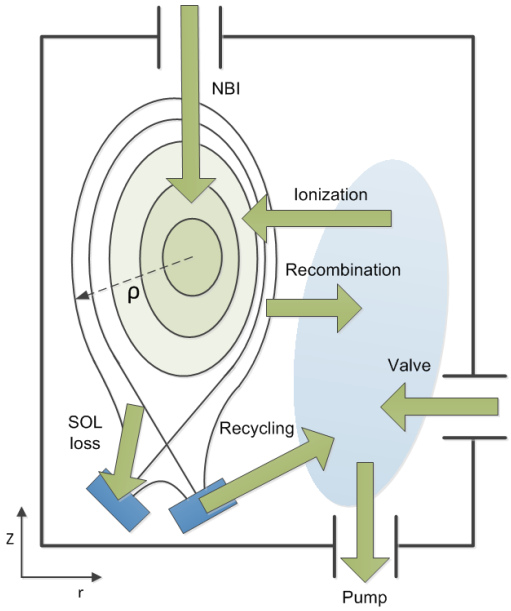


Fig. 1. Schematic representation of the tokamak cross-section in the $r$-$Z$ plane. Depicted are the plasma, the wall components, the neutral vacuum and the modeled particle flows.

### A. Physics-based model of plasma particle transport

The evolution of the electron density $n_e(\rho,t)$ resulting from radial (1D) transport is modeled by a PDE [6] on the domain $\Omega = \{(t,\rho) \in \mathbb{R} \mid t_0 \le t \le t_f,\ 0 \le \rho \le \rho_e\}$, where $\rho(r,Z) \in \mathcal{S} := \{f : \Theta \to [0,\rho_e]\}$ is a measure for radial distance from the plasma center and $r, Z \in \Theta = [r_{min}, r_{max}] \times [Z_{min}, Z_{max}]$ is the two-dimensional space of the tokamak poloidal cross-section.

$$\frac{1}{V'}\frac{\partial}{\partial t}\left(n_e V'\right) + \frac{1}{V'}\frac{\partial \Gamma}{\partial \rho} = S \tag{1}$$

where $S(\rho,t)$ is the net electron source and $V' = \frac{\partial V}{\partial \rho} \in \mathcal{V} := \{f : [0,\rho_e] \to \mathbb{R}^+\}$ is the derivative of the volume enclosed by a surface of constant $\rho$.

*1) Radial transport:* Radial transport $\Gamma(\rho,t)$ is governed by diffusion and a drift velocity [6], [15] and is given by

$$\Gamma = -V'\left(G_1 \chi \frac{\partial n_e}{\partial \rho} + G_2 \nu n_e\right) \tag{2}$$

where $\chi = \chi(\rho, c_{lh})$ and $\nu = \nu(\rho, I_p, c_{lh})$ are the coefficients of radial diffusion and drift, and $G_1(\rho(r,Z))$ and $G_2(\rho(r,Z))$ are geometrical coefficients. The drift coefficient $\nu$ is assumed to be proportional to the plasma current $I_p$, i.e. $\nu \propto I_p$, to model the increase of pinch at higher current. In many tokamaks, sufficient heating of the plasma causes an abrupt transition to higher confinement of the plasma energy and density, called an H-mode [16]. An H-mode ($c_{lh} = 1$) implies a reduction of transport in the plasma

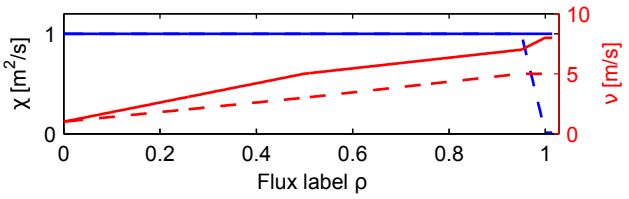


Fig. 2. Modeled diffusion $\chi$ (blue) and drift $\nu$ (red) coefficients as a function of $\rho$. Solid and dashed lines indicate the coefficients for low confinement ($c_{lh} = 0$) and high confinement ($c_{lh} = 1$), respectively.

edge [17] and is reproduced by a lower diffusion coefficient at the edge and a higher drift velocity, see Figure 2.

*2) Domain and boundary conditions:* The domain edge $\rho_e$ is chosen as $\rho_e = 1 + \lambda_{SOL}$ where the constant $\lambda_{SOL}$ is the dimensionless scrape-off layer width [16]. The boundary conditions are $\frac{\partial n_e}{\partial \rho}\Big|_{\rho=0} = 0$ and $n_e|_{\rho=\rho_e} = 0$. The outflux at the domain edge $\Gamma|_{\rho=\rho_e}$ is treated as a source to the vacuum.

*3) Sources:* The plasma source $S(\rho, t)$ consists of multiple sources and sinks that are linked to the wall and vacuum inventories, as depicted in Figure 1, and is modeled as

$$S = \Lambda_{NBI}\Gamma_{NBI}(t) - S_{SOL} + S_{ion} - S_{rec} \tag{3}$$

where $\Gamma_{NBI}(t)$ is the neutral beam injection fuelling rate. The scrape-off layer sink is modeled as $S_{SOL} = \frac{H(\rho-1)n_e}{\tau_{SOL}}$ where $H(\cdot)$ is the Heaviside function and $\tau_{SOL}(c_{ld})$ is the scrape-off layer loss time constant. The ionization source and recombination sink are modeled as $S_{ion} = \langle\sigma v\rangle_{ion}\Lambda_{ion}\frac{N_v}{V_r - V_p}n_e$ and $S_{rec} = \langle\sigma v\rangle_{rec}\Lambda_{rec}n_e^2$, where $V_r$ is the tokamak vessel volume, $V_p = \int_0^{\rho_e} V' d\rho$ is the plasma volume, and $\langle\sigma v\rangle_{ion}(T_{e,b})$ and $\langle\sigma v\rangle_{rec}(T_{e,b})$ are the cross-sections for ionization and recombination [16]. The functions $\Lambda_{NBI}(\rho)$, $\Lambda_{ion}(\rho, c_{ld})$ and $\Lambda_{rec}(\rho, c_{ld})$ are spatial distributions of neutral beam injection, ionization and recombination, see Figure 3(b). These are chosen ad-hoc in this study but can be computed using more detailed physics models. The evolution of the wall inventory $N_w(t)$ is modeled as

$$\frac{dN_w}{dt} = \Gamma_{SOL} - \Gamma_{recycling} \tag{4}$$

where $\Gamma_{recycling} = \frac{N_w}{\tau_{release}} + \frac{N_w}{N_{sat}}\Gamma_{SOL}$, $\Gamma_{SOL} = \int_{V_p} S_{SOL} dV$, $\tau_{release}$ is the wall inventory loss time constant and $N_{sat}(c_{ld}, c_{lh})$ is the saturation level for the wall inventory. The evolution of the vacuum inventory $N_v(t)$ is modeled as

$$\frac{dN_v}{dt} = \int_{V_p}(S_{rec} - S_{ion})\,dV + \Gamma_{recycling} + \Gamma|_{\rho=\rho_e} - c_{pump}\frac{N_v}{V_v} + \Gamma_{valve}(t) \tag{5}$$

where the constant $c_{pump}$ expresses the proportionality between the vacuum density and the pump outflow.

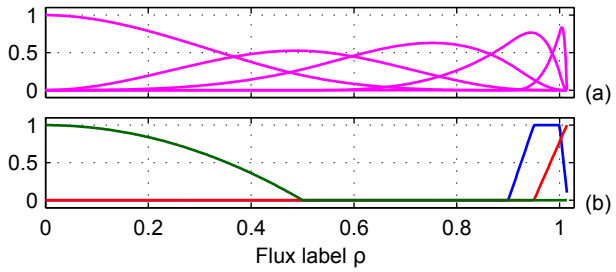


Fig. 3. Example of basis functions $\Lambda_\alpha$ in (a) and spatial distributions $\Lambda_{ion}$ (blue), $\Lambda_{rec}$ (red) and $\Lambda_{NBI}$ (green) for limited plasma ($c_{ld} = 0$) in (b).

### B. Inputs

The gas injection inflow rate $\Gamma_{valve}(t)$ and neutral beam injection rate $\Gamma_{NBI}(t)$ are considered as inputs. They are constrained to be nonnegative and have limits, expressed as

$$0 \le \Gamma_{valve}(t) \le \Gamma_{valve}^{upper} \tag{6a}$$
$$0 \le \Gamma_{NBI}(t) \le \Gamma_{NBI}^{upper} \tag{6b}$$

We assume that, within these constraints, the inputs are either proportional to the actuator input voltage, or that the actuators are feedback controlled to provide $\Gamma_{valve}(t)$ and $\Gamma_{NBI}(t)$ at time $t \in \mathbb{R}_{\ge t_0}$.

### C. Exogeneous parameter

To evaluate the model (1)-(5), we require real-time knowledge of certain plasma quantities that were introduced before. We define the time-varying parameter $p(t) \in \mathcal{P}$ as

$$p = \begin{bmatrix} T_{e,b} & I_p & \rho(r,Z) & V' & c_{ld} & c_{lh} \end{bmatrix} \tag{7}$$

where $\mathcal{P} = \{\mathbb{R}^2 \times \mathcal{S} \times \mathcal{V} \times \{0,1\}^2\}$ is the parameter space.

### D. Numerical evaluation using a finite element method

The electron density is discretized in space using finite elements and is written as

$$n_e(\rho, t) = \sum_{\alpha=1}^{m} \Lambda_\alpha(\rho)\, b_\alpha(t) \tag{8}$$

We choose the basis functions $\Lambda_\alpha : [0, \rho_e] \to \mathbb{R}$, $\alpha = 1, 2, ..., m$, as cubic B-splines with a finite support [18]. For the purpose of control and observer design, we choose a small number of states ($m = 5$), with closely-spaced spline knots around the plasma edge, see Figure 3(a). The variables $b(t) = \begin{bmatrix} b_1(t) & \cdots & b_m(t) \end{bmatrix}^T$ are the time-varying spline coefficients. The boundary conditions are satisfied by choosing an appropriate basis function set such that $\frac{\partial \Lambda_\alpha}{\partial \rho}\Big|_{\rho=0} = 0$, $\Lambda_\alpha(\rho_e) = 0$, $\alpha = 1, ..., m$.

Projecting the PDE (1) onto a set of test functions $\Psi_\alpha : [0, \rho_e] \to \mathbb{R}$, $\alpha = 1, 2, ..., m$ with $\sum_{\alpha=1}^{m} \Psi_\alpha(\rho) = 1$, $\rho \in [0, \rho_e]$ yields the weak form of the PDE (1). This reduces (1), (4) and (5) to a system of nonlinear ODEs, given by

$$\frac{dx}{dt} = f(p, x) + \begin{bmatrix} 0 & P \\ 0 & 0 \\ 1 & 0 \end{bmatrix} u \tag{9}$$

where $P \in \mathbb{R}^{m\times 1}$, and the state $x(t) \in \mathbb{R}^{n_x}$ and the input $u(t) \in \mathbb{R}^{n_u}$ are defined as

$$x(t) = \begin{bmatrix} b(t) \\ N_w(t) \\ N_v(t) \end{bmatrix} \qquad u(t) = \begin{bmatrix} \Gamma_{valve}(t) \\ \Gamma_{NBI}(t) \end{bmatrix}$$

where $n_x = m + 2$, $n_u = 2$ and

$$f(p,x) = W(p)\,x + \begin{bmatrix} f_b(p,b,N_v) \\ f_w(p,b,N_w) \\ f_v(p,b,N_w,N_v) \end{bmatrix}$$

where $W : \mathcal{P} \to \mathbb{R}^{n_x \times n_x}$, and $f_b : \mathcal{P} \times \mathbb{R}^m \times \mathbb{R} \to \mathbb{R}^m$, $f_w : \mathcal{P} \times \mathbb{R}^m \times \mathbb{R} \to \mathbb{R}$, $f_v : \mathcal{P} \times \mathbb{R}^m \times \mathbb{R} \times \mathbb{R} \to \mathbb{R}$ are quadratic or bilinear functions in $b$, $N_w$ and $N_v$. We choose an equidistant time discretization $t_k = t_0 + kT_s,\ k \in \{0,1,...,N\}$ where $T_s > 0$ is the time step and $N = (t_f - t_0)/T_s \in \mathbb{N}$. The discrete-time input, state, parameter and output are defined as $u_k := u(t_k)$, $x_k := x(t_k)$, $p_k := p(t_k)$, $y_k := y(t_k)$, respectively. We apply a first-order approximation of the time derivative $\dot{x}(t_k) \approx (x_{k+1} - x_k)/T_s$ and trapezoidal method[1] $f(x(t_k)) \approx \theta f(x_{k+1}) + (1-\theta) f(x_k)$ where $\theta \in [0,1]$ is a discretization parameter. We choose $\theta = \frac{1}{2}$. Applying the time discretization on (9) yields the discrete-time state-space equation

$$x_k = f_d(p_{k-1}, x_{k-1}) + Bu_{k-1} \tag{10}$$

where $f_d : \mathcal{P} \times \mathbb{R}^{n_x} \to \mathbb{R}^{n_x}$ and $B \in \mathbb{R}^{n_x \times n_u}$.

### *E. Measurements*

The interferometry measurement output $\Delta\phi$ is proportional to the line-integrated electron density along one or more laser chords intersecting the plasma (see e.g. [3]). The fringe jump magnitude equals an integer multiple of $2\pi$. The interferometry phase signal $\Delta\phi(t) \in \mathbb{R}$ at time $t_k$ at the $c$-th chord is denoted by $\Delta\phi_k^c$ and is given by

$$\Delta\phi_k^c = c_{FIR} \int_{L_c} n_e(\rho(r,Z), t_k)\, dL + 2\pi d_k^c \tag{11}$$

where $c_{FIR}$ is the interferometry constant, $L_c$ is the intersection length of the plasma and the $c$-th laser chord and $d_k^c \in \mathbb{N}$ is the number of fringe jumps at time $t_k$ on the $c$-th chord. By stacking individual output signals (11), the measurement output vector of all $n_{FIR}$ interferometry chords can be represented as $y_k \in \mathbb{R}^{n_{FIR}}$ and is given by

$$y_k = \begin{bmatrix} \int_{L_1} n_e(\rho(r,Z), t_k)\, dL \\ \vdots \\ \int_{L_{n_{FIR}}} n_e(\rho(r,Z), t_k)\, dL \end{bmatrix} + \delta d_k \tag{12}$$

where $\delta = \frac{2\pi}{c_{FIR}}$ and $d_k = \begin{bmatrix} d_k^1 & \cdots & d_k^{n_{FIR}} \end{bmatrix}^T \in \mathbb{N}^{n_{FIR}}$ is the number of fringe jumps at time $t_k$. Integer jumps can be represented as $d_k^c = d_{k-1}^c + \Delta_{k-1}^c$ where $\Delta_k^c \in \mathbb{N}$ is a stochastic variable. The fringe jump state equation is given by

$$d_k = d_{k-1} + \Delta_{k-1},\ k \in \{1,2,...,N\} \tag{13}$$

where $\Delta_k = \begin{bmatrix} \Delta_k^1 & \cdots & \Delta_k^{n_{FIR}} \end{bmatrix}^T \in \mathbb{N}^{n_{FIR}}$, $k \in \{0,1,...,N-1\}$. The probability of jumps is known to be strongly correlated with fast changes of the plasma density [1], [14], but obtaining the probability density function for $\Delta_k$, $k \in \{0,1,...,N-1\}$ is difficult and beyond the scope of this paper. Yet we assume that the elements of $\Delta_k$ are independent and identically distributed, that $d_{k=1} = 0^{n_{FIR}}$ and that the expected value $\mathbb{E}[\Delta_k] = 0$, $k \in \{1,2,...,N-1\}$.

The spatial discretization (8) allows to write the line integrals (12) as a linear combination of the state $x$. The output of the state-space system is written as

$$y_k = C(p_k)\, x_k + \delta d_k \tag{14}$$

where $C(p_k) = \begin{bmatrix} \Omega(p_k) & 0^{n_{FIR}\times 2} \end{bmatrix}$ and $\Omega_{ij}(p_k) = \int_{L_i} \Lambda_j(\rho(r,Z))\, dL$, $i \in \{1,2,...,n_{FIR}\}, j \in \{1,2,...,m\}$, is numerically evaluated using $\rho(r,Z)$, which is assumed to be available from real-time 2D equilibrium reconstruction.

The computation of the matrices in (10) and (14) with $n_x = 7$ and $n_{FIR} = 14$ takes 2 ms per time step in MATLAB using an Intel®Core™2 DUO E6600 at 2.40 GHz PC running Windows 7. We emphasize that this is computationally the most expensive compared to the observer and controller equations. Future implementation on a tokamak control system could easily reduce the computations to below the typical sampling time of 1 ms. Note that the typical control bandwidth is below 25 Hz [2].

### *F. TCV tokamak simulation: model validation*

We present a simulation of the model (10), (14) and compare it with measurement data from the TCV tokamak. We use the parameter and input signals from TCV shot #41953 to recreate the discharge. The model coefficients are chosen to be representative for a typical TCV discharge. The gas injection system is used for actuation while the neutral beam is not. In Figure 4, the measurements and simulation results are shown. During flat-top, there is a good agreement between the measurements and the simulated data (Fig. 2.1(b)(d)). However, the model is not accurate during ramp-up, ramp-down and mode transitions. Obtaining more accurate simulations for these situations would require better models for (3)-(5), but this is difficult since wall saturation and recycling are highly complex and nonlinear physical processes and depend on the time history of the tokamak. Still, the model provides insight in the dynamical behaviour and can be used for controller and observer design since it represents the most dominant behaviour.

## III. OBSERVER DESIGN BASED ON EXTENDED KALMAN FILTERING

We use an observer to estimate the plasma density, which fuses measurements (14) with a model of the dynamical system (10), (13) to produce state estimates. An extended

[1]This is a generalization of the trapezoidal rule. $\theta = \frac{1}{2}$ yields the trapezoidal rule, whereas $\theta = 0$ and $\theta = 1$ yield the forward and backward Euler method, respectively. For practical reasons, we apply the approximations $p_{k+1} \approx p_k$ and $u_{k+1} \approx u_k$. To obtain the most stable numerical scheme that requires no iterations, we choose $f(x_{k+1}) \approx W x_{k+1} + \left[ f_b(b_k, N_{v,k+1})^T \ f_w(b_k, N_{w,k+1}) \ f_v(b_k, N_{w,k+1}, N_{v,k+1}) \right]^T$.

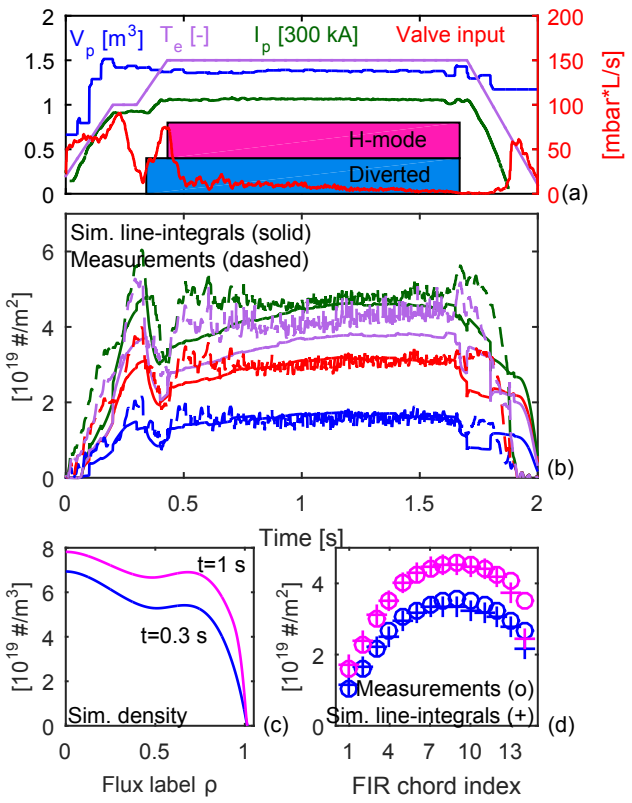


Fig. 4. Nominal simulation of a TCV discharge, using parameter and input data from TCV shot #41953 shown in (a). The simulated line-integrated density (solid) and measurements from TCV shot #41953 (dashed) are shown in (b). The simulated density profiles at $t = 0.3s$ (blue) and $t = 1s$ (magenta) are shown in (c). The simulated line-integrated density and measurement at these time slices are shown in (d).

Kalman filter [19] is designed to produce estimates $\hat{x}_{k|k}$ of the state $x_k$, $k \in \{1, 2, ..., N\}$. An additive random-walk state disturbance is introduced, which allows to capture and estimate modeling errors. Furthermore, we introduce a novel approach to detecting fringe jumps based on the measurement residual.

### A. Kalman filter for estimation of state and disturbances

We assume that the output $y_k$ in (14) is corrupted by white measurement noise $v_k \sim \mathcal{N}(0, R_k)$ and the state $x_k$ in (10) is subject to process noise $w_k^x \sim \mathcal{N}(0, Q_k^x)$. We add unknown disturbances $\zeta_k \in \mathbb{R}^m$ to the density states to represent unmodeled dynamics. The disturbance is assumed to be a random-walk noise $\zeta_{k+1} = \zeta_k + w_k^\zeta$, where $w_k^\zeta \sim \mathcal{N}\left(0, Q_k^\zeta\right)$. The augmented system is written as

$$x_k = f_d(p_{k-1}, x_{k-1}) + B_d\zeta_{k-1} + Bu_{k-1} + w_{k-1}^x \quad (15a)$$
$$\zeta_k = \zeta_{k-1} + w_{k-1}^\zeta \quad (15b)$$
$$d_k = d_{k-1} + \Delta_{k-1} \quad (15c)$$
$$y_k = C(p_k)\, x_k + \delta d_k + v_k \quad (15d)$$

with $B_d = \begin{bmatrix} I^{m\times m} & 0^{m\times 2} \end{bmatrix}^T$ such that each disturbance entry influences one element of the density state. The augmented state $\boldsymbol{x}_k \in \mathbb{R}^{n_x+m}$ is defined as $\boldsymbol{x}_k = \begin{bmatrix} x_k^T & \zeta_k^T \end{bmatrix}^T$.

By defining

$$F_k = \begin{bmatrix} \frac{\partial f_d}{\partial x_k}\Big|_{p_k, \hat{x}_{k|k}} & B_d \\ 0 & I^{m\times m} \end{bmatrix} \quad G = \begin{bmatrix} B \\ 0 \end{bmatrix}$$

$$H_k = \begin{bmatrix} C(p_k) & 0 \end{bmatrix} \quad Q_k = \begin{bmatrix} Q_k^x & 0 \\ 0 & Q_k^\zeta \end{bmatrix}$$

we can write the extended Kalman filter [19] for (15) as[2]

$$\hat{\boldsymbol{x}}_{k|k-1} = F_{k-1}\hat{\boldsymbol{x}}_{k-1|k-1} + Gu_{k-1} \quad (16a)$$
$$P_{k|k-1} = F_{k-1}P_{k-1|k-1}F_{k-1}^T + Q_{k-1} \quad (16b)$$
$$z_k = y_k - H_k\hat{\boldsymbol{x}}_{k|k-1} - \delta\hat{d}_{k-1} \quad (16c)$$
$$L_k = P_{k|k-1}H_k^T\left(H_kP_{k|k-1}H_k^T + R_k\right)^{-1} \quad (16d)$$
$$\hat{\boldsymbol{x}}_{k|k} = \hat{\boldsymbol{x}}_{k|k-1} + L_k\left(z_k - \delta\mathbb{E}\left[\Delta_{k-1} \mid z_k\right]\right) \quad (16e)$$
$$\hat{d}_k = \hat{d}_{k-1} + \mathbb{E}\left[\Delta_{k-1} \mid z_k\right] \quad (16f)$$
$$P_{k|k} = \left(I - L_kH_k\right)P_{k|k-1} \quad (16g)$$

where $P_{k|k}$ is the covariance matrix of the estimate $\hat{\boldsymbol{x}}_{k|k}$, $z_k$ is the innovation residual and $L_k$ is the (suboptimal) Kalman gain. By estimating the disturbance $\zeta_k$, the Kalman filter effectively compensates for systematic modeling errors.

Since the probability distribution of fringe jumps $\Delta_k$ is unknown, we propose to detect and correct for fringe jumps from the innovation residual $z_k$ using a heuristic threshold method. We choose detection intervals for $z_k$, such that excursions of $z_k^c$ outside $\pm\gamma\delta$ are flagged as a fringe jump of appropriate magnitude $\Delta_k^c \in \mathbb{N}$, where $z_k^c$ is the $c$-th element of $z_k$ and $\gamma \in (0, 1)$ determines the detection sensitivity. The detected jump on chord $c$, $c = 1, ..., n_{FIR}$, is denoted by $\mathbb{E}\left[\Delta_{k-1}^c \mid z_k\right]$ and is chosen as

$$\mathbb{E}\left[\Delta_{k-1}^c \mid z_k\right] \approx \operatorname{sgn}\left(\frac{z_k^c}{\delta}\right)\left\lceil\left|\frac{z_k^c}{\delta}\right| - \gamma\right\rceil \quad (17)$$

where $\lceil a \rceil$ is the smallest integer larger then or equal to $a \in \mathbb{R}$. In practice we choose $\gamma = 0.9$. The detected jump (17) is substracted from the innovation residual in (16e).

### B. Design of the covariance matrices

The performance, accuracy and stability of the extended Kalman filter is determined by the choice of the covariance matrices $Q_k^x$, $Q_k^\zeta$ and $R_k$, $k \in \{0, 1, ..., N-1\}$. We choose the measurement covariance matrix $R_k$ a priori as the sample covariance of high-pass measurements, but increase the covariance on output channels we distrust or whose numerical evaluation of the line-integrals (as discussed in Section II-E) are sensitive to errors in the equilibrium reconstruction. In this way, the Kalman filter will rely less on interferometry chords deemed unreliable. The process covariance matrix $Q_k^x$ is chosen as a symmetric Toeplitz matrix with a descending first row. The entries reflect the amount of uncertainty on the state evolution. The estimation accuracy can be improved

[2]Note that the prediction $\hat{\boldsymbol{x}}_{k|k-1} = \mathbb{E}\left[\boldsymbol{x}_k \mid y^{k-1}\right] = \mathbb{E}\left[F_{k-1}(x_{k-1})\,\boldsymbol{x}_{k-1} + Gu_{k-1} \mid y^{k-1}\right]$ where $y^k = (y_1, y_2, ..., y_k)$, $k \in \{1, 2, ..., N\}$, is approximated for practical reasons by (16a), i.e. $\hat{\boldsymbol{x}}_{k|k-1} \approx F_{k-1}\left(\hat{x}_{k-1|k-1}\right)\hat{\boldsymbol{x}}_{k-1|k-1} + Gu_{k-1}$.

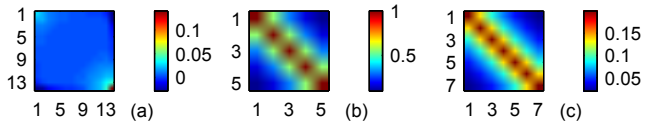


Fig. 5. Graphical representation of the matrices $R_k$ (a), $Q^T$ (b) and $Q_k^x$ (c).

TABLE I
MODEL PERTURBATIONS

| Coefficient | Unit | Nominal value | Perturbed value |
|---|---|---|---|
| $\chi$ | $[m^2/s]$ | 1 | 0.8 |
| $\nu$ | $[m/s]$ | 10 | 5 |
| $N_{sat}$ | $[-]$ | $3 \times 10^{19}$ | $6 \times 10^{19}$ |
| $\langle \sigma v \rangle_{ion}(T_e)$ | $[m^3/s]$ | $1 \times 10^{-14}$ | $2 \times 10^{-14}$ |

by increasing $Q_k^x$, thereby generating a higher Kalman gain $L_k$, although this also causes the observer to amplify measurement noise in the estimate. The disturbance covariance matrix $Q_k^\zeta$ is chosen as the product of a diagonal matrix $Q_D$ and a symmetric Toeplitz matrix $Q_T$ with a descending first row. The latter promotes spatial smoothness of the disturbances [5]. The rate at which estimates of the state disturbance $\hat{\zeta}_k$ change and thereby compensate for modeling errors is increased by increasing the state disturbance covariance matrix $Q_k^\zeta$.

### C. Observer performance to simulated data

*1) Response to model perturbations:* In order to show the observer performance, we simulate the system (9) and apply the observer (16) with perturbed model coefficients (see Table I) to the simulation output (14). The simulation uses input and parameter data from TCV shot #41953 to recreate a realistic discharge scenario. White noise with covariance equal to the sample covariance of high-pass measurements of TCV shot #41953 is added to (14) as measurement noise. The simulation results are shown in Figure 6. As desired, the estimation error is small and the disturbance estimate $\hat{d}_k$ compensates for systematic modeling errors, formed by the perturbed coefficients.

*2) Response to different number of outputs:* The number of interferometry channels $n_{FIR}$ is different for each tokamak. Existing density reconstruction methods require $m \leq n_{FIR}$ to invert $\Omega(p_k)$ in (14) and provide the instantaneous mapping $y_k \rightarrow \hat{x}_k$. We apply the observer (16) with $m = 5$ on the system simulation from Section III-C.1 for different subsets of the 14 interferometry channels of TCV. In Figure 7, the observer performance is shown using either a central channel, a side channel, three channels, and all 14 channels. In case of using a single channel, the profile shape is entirely deduced from the model known to the observer. Consequently, the accuracy is poor. While 14 output channels provide the best accuracy, only three channels already provide good accuracy and a small steady-state estimation error.

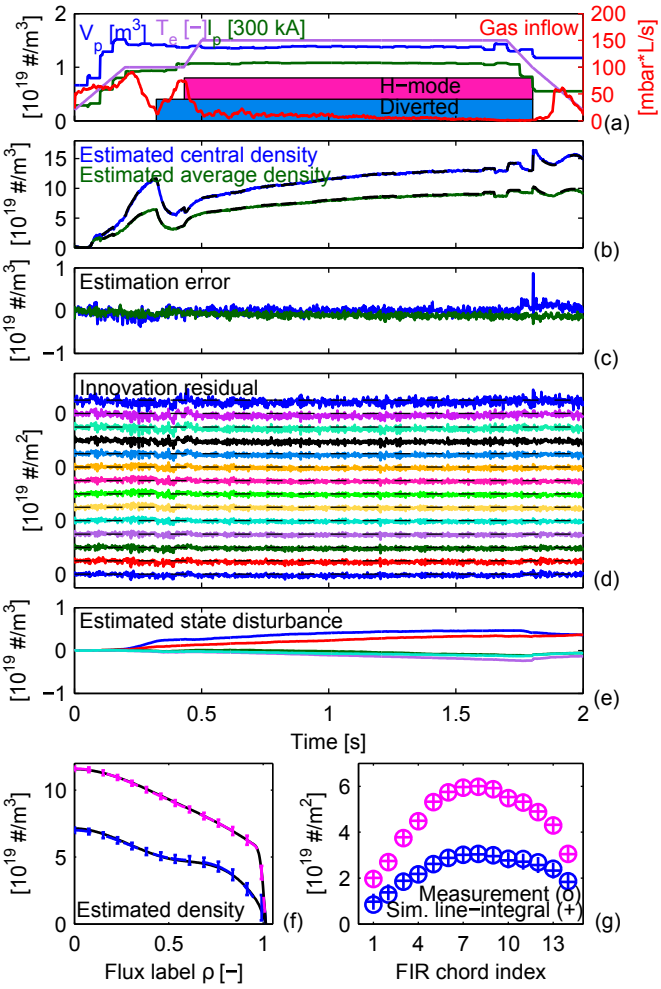


Fig. 6. Observer results for simulated data with perturbed model coefficients, using parameter and input data from TCV shot #41953 shown in (a). The estimated central and average density (solid) are shown in (b), with the respective simulated quanties in black. The elements of the innovation residual (16c) are shown in (c), individually offset at intervals of $1 \times 10^{19}$. The estimated disturbance is shown in (d). The simulated and estimated density profiles with confidence bounds at $t = 0.25$ (blue) and $t = 0.7$ (magenta) are shown in (f). The simulated and estimated measurements at these time slices are shown in (g).

### D. Observer performance to experimental measurement data

The performance of the observer on measurement data from TCV shot #47675 is shown in Figure 8. This shot contains two consecutive fringe jumps. All 14 channels except three malfunctioning chords are used to estimate the density. The results show good estimation accuracy. While a double fringe jump around $t = 0.33$ is correctly flagged and corrected (see Figure 8(f)), spatial discrepancies in the innovation residual around $t = 0.42$ and $t = 0.53$ (see Figure 8(c)(f)) exceed the detection threshold (17) and are therefore incorrectly flagged as jumps. We assign the latter to inaccurate evaluation of the line integrals (see Section II-E) due to inaccurate information of $\rho(r, Z)$. Still, these false alerts do not lead to unrealistic estimates of the density, as is observed in Figure 8(b)(e).

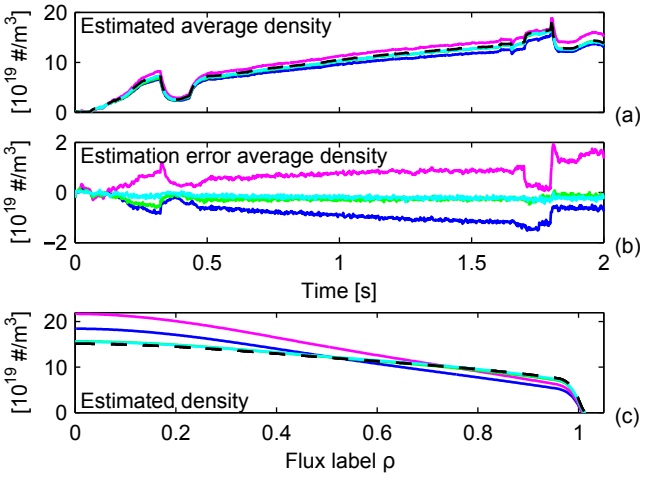


Fig. 7. Observer response for simulated data to different numbers of measurement channels. The simulated density is shown as a black dashed line. Estimated average densities (a) using either central channel #7 (blue), side channel #11 (magenta), three channels #3,#7,#11 (green), all 14 channels (cyan). The estimation error in average density (b). The profiles at $t = 1$ are shown in (c).

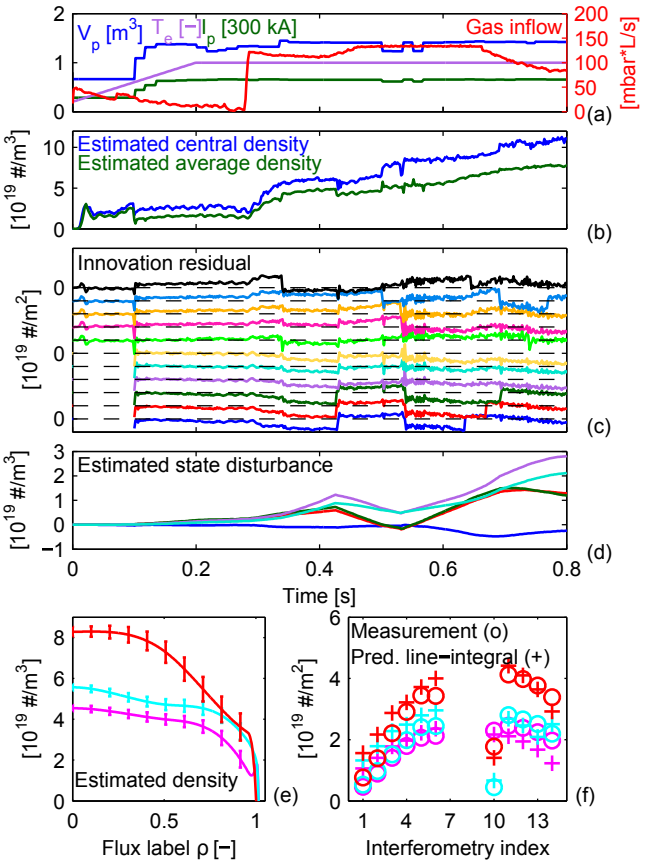


Fig. 8. Observer results for experimental data of TCV shot #47675. The input and parameter data of TCV shot #47675 are shown in (a). The estimated central and average are shown in (b). The elements of the innovation residual (16c) are shown in (c), individually offset at intervals of $1 \times 10^{19}$. The estimated disturbance is shown in (d). The estimated density profiles with confidence bounds at $t = 0.32$ (magenta), $t = 0.35$ (light blue) and $t = 0.55$ (red) are shown in (e). The measurements and predicted measurements at these time slices are shown in (f).

TABLE II
MODEL UNCERTAINTIES

| Coefficient | Unit | Nominal value | Uncertainty |
|---|---|---|---|
| $\chi$ | $[m^2/s]$ | 1 | $\pm 20\%$ |
| $\nu\,(c_{lh}=0)$ | $[m/s]$ | 10 | $\pm 20\%$ |
| $\nu\,(c_{lh}=1)$ | $[m/s]$ | 5 | $\pm 20\%$ |
| $\tau_{SOL}\,(c_{lh}=0)$ | $[s^{-1}]$ | $4 \times 10^{-5}$ | $\pm 50\%$ |
| $\tau_{SOL}\,(c_{lh}=1)$ | $[s^{-1}]$ | $8 \times 10^{-5}$ | $\pm 50\%$ |
| $N_{sat}$ | $[-]$ | $3 \times 10^{19}$ | $\pm 50\%$ |
| $\langle \sigma v \rangle_{ion}\,(T_e)$ | $[m^3/s]$ | $1 \times 10^{-14}$ | $\pm 20\%$ |
| $I_p$ | $[A]$ | $300 \times 10^3$ | $\pm 10\%$ |

## IV. ROBUST CONTROL DESIGN

We propose to use robust $H_\infty$ control synthesis [20] for designing a switched feedback tracking controller for the plasma density. This model-based approach could improve the controller design since nonlinearities and time history of the system complicate the identification of the dynamics from measurement data. By choosing the uncertainty bounds sufficiently large, we attempt to synthesize controllers that are stable despite model mismatches, nonlinearities and inaccurate parameter information. Since the dynamics vary substantially in different modes, we propose to use a switching controller for each combination of $c_{ld}$ and $c_{lh}$. In this paper we consider control of one variable, namely the average plasma density. MIMO control of the density profile requires suitable actuators but can also be realized with this method.

A full discussion of the design procedure exceeds the limitations of this paper. Instead we will briefly describe the design steps involved and show simulation results of the interconnection of the observer and controller. We emphasize that our main contribution in feedback control of the density is the use of an observer in the closed-loop interconnection.

### A. Controller design procedure

We embed the system (10) in a uncertain plant model with uncertain parameter $p = \overline{p} + \Delta p$, model coefficients $c = \overline{c} + \Delta c$ and density state $x = \overline{x} + \Delta x$ as listed in Table II. Because of the switching on $c_{ld}$ and $c_{lh}$, we do not regard uncertainty due to $c_{ld}$ and $c_{lh}$. The controlled variable is the average density $x_c\,(t) = \frac{1}{V_p} \int_{V_p} n_e dV$, the control input is the gas injection $u_{valve}\,(t)$ and the tracking error is defined as $e = r - x_c$ where $r$ is the reference. To impose reference tracking up to the bandwidth $\omega_b = 4$ Hz, zero steady-state error and disturbance rejection, we augment the plant with suitable weighting filters. Using the MATLAB Robust Control Toolbox, we synthesize switched linear controllers

$$u_{valve} = K_{c_{ld},c_{lh}}\,(s)\,e \qquad c_{ld} \in \{0,1\} \quad c_{lh} \in \{0,1\} \quad (18)$$

that stabilize the closed-loop interconnection and achieve robust performance against the uncertainties. We switch controllers $K_{c_{ld},c_{lh}}\,(s)$ based on real-time knowledge of $c_{ld}$ and $c_{lh}$, and we assume that the switched closed-loop system is stable. The latter is plausible since inter-event times of switching exceed the transients induced by switching. An

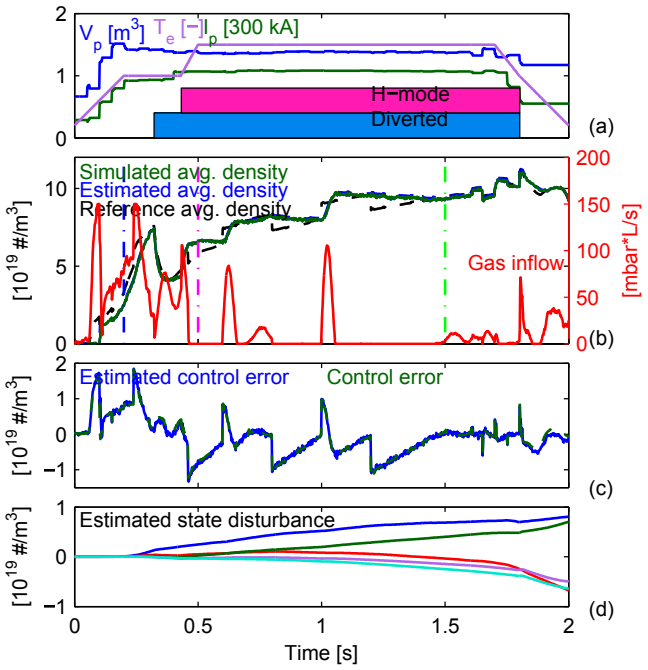


Fig. 9. Closed-loop performance for a high density H-mode shot. Positive steps in the reference are accurately tracked, but negative steps are not tracked: the actuator closes and the density decays autonomously.

anti-windup system is used to withhold the integral action from winding up if the input $u_{valve}$ reaches its limits (6).

### B. Closed-loop simulation

The feedback controller (18) is designed for a high-density discharge which transitions from limiter to divertor, and from low- to high-confinement mode and vice versa. The reference is a typical trajectory of the average density, plus a number of positive and negative steps. The simulation results can be seen in Figure 9. To display the closed-loop performance, certain model coefficients in the observer and controller are perturbed, see Table I. As desired, the disturbance estimate $\hat{\zeta}_k$ compensates for these perturbations. The controller is able to quickly compensate for positive steps in the reference as desired, but not to negative steps due to the nonnegativity constraint in the input (6).

## V. CONCLUSIONS AND FUTURE WORKS

We have introduced a systematic model-based approach to the design of an observer-based robust feedback controller for the plasma density in tokamaks. A control-oriented model was derived from a spatially discretized transport PDE which takes the influence of physical plasma quantities into account. Simulation results show that the model provides good approximations of the density in a tokamak discharge. Based on this model, an extended Kalman filter was used to estimate the density profile and disturbances. Observer simulations on experimental data show that the observer estimates the density profile with a high accuracy. Finally, $H_\infty$ control synthesis was used to design switched robust state feedback controllers. The interconnection of the observer and the controller was tested in simulation, which showed good tracking performance. The tracking performance is predominantly limited by the nonnegativity constraint in the inputs.

In future studies, additional measurements may be incorporated for an even better profile estimate. The detection of fringe jumps can be improved by incorporating the measurement residuals of neighbouring interferometry chords. Ultimately, the observer-based controller will be tested on more detailed physics models and implemented on tokamak control systems.

## REFERENCES


[1] A. Mlynek, *et al.*, "Real-time feedback control of the plasma density profile on ASDEX Upgrade," *Nuclear Fusion*, vol. 51, no. 4, p. 043002, 2011. [Online]. Available: http://stacks.iop.org/0029-5515/51/i=4/a=043002

[2] W. Vijvers, *et al.*, "Non-linear digital real-time control in the TCV tokamak," in *39th EPS Conference on Plasma Physics 2012 (EPS 2012) and the 16th International Congress on Plasma Physics*, 2012.

[3] I. H. Hutchinson, *Principles of Plasma Diagnostics*. Cambridge University Press, 2005.

[4] D. Moreau, *et al.*, "Plasma models for real-time control of advanced tokamak scenarios," *Nuclear Fusion*, vol. 51, p. 063009, 2011.

[5] F. Felici, M. de Baar, and M. Steinbuch, "A dynamic state observer for real-time reconstruction of the tokamak plasma profile state and disturbances," in *American Control Conference (ACC), 2014*, June 2014, pp. 4816–4823.

[6] F. Hinton and R. Hazeltine, "Theory of plasma transport in toroidal confinement systems," *Review of Modern Physics*, vol. 48, pp. 239–308, 1976.

[7] G. V. Pereverzev and P. N. Yushmanov, "ASTRA. Automated System for TRansport Analysis in a tokamak," IPP Report, Tech. Rep. 5/98, 2002.

[8] L. Schmitz, *et al.*, "Plasma and neutral dynamic in a simulated tokamak gas target divertor," *Physics of Plasmas*, vol. 2, no. 8, pp. 3081–3094, 1994.

[9] P. Tamain, *et al.*, "Thermal interaction of plasma with gas puffing," *Journal of Nuclear Materials*, vol. 363-365, pp. 844–848, 2007.

[10] J. Artaud, *et al.*, "The CRONOS suite of codes for integrated tokamak modelling," *Nuclear Fusion*, vol. 50, no. 4, p. 043001, 2010. [Online]. Available: http://stacks.iop.org/0029-5515/50/i=4/a=043001

[11] G. Maddison, *et al.*, "Global modelling of tank gas density and effects on plasma density control in MAST," *Plasma Physics and Controlled Fusion*, vol. 48, pp. 71–107, 2006.

[12] A. Murari, *et al.*, "Real-time recovery of the electron density from interferometric measurements affected by fringe jumps," *Review of Scientific Instruments*, vol. 77, p. 073505, 2006.

[13] L. Zabeo, *et al.*, "Different approaches to real time correction of fringe jumps in interferometers for nuclear fusion," *Review of Scientific Instruments*, 2004.

[14] C. Gil, *et al.*, "Analysis of the JET FIR interferometer beam phase changes during plasmas and application for fast fringe jump corrections by electronics," *Journal of Physics: Conference Series*, vol. 227, p. 012032, 2010.

[15] A. Zabolotsky, *et al.*, "Influence of particle sources on electron density peaking in TCV and JET," *Nuclear Fusion*, vol. 46, pp. 594–607, 2006.

[16] J. A. Wesson, *Tokamaks*, 3rd ed. Oxford University Press, 2004.

[17] M. Willensdorfer, *et al.*, "Particle transport analysis of the density build-up after the L-H transition in ASDEX Upgrade," *Nuclear Fusion*, vol. 53, no. 8, 2013.

[18] C. de Boor, *A practical guide to splines*, ser. Applied Mathematical Science. Springer-Verlag, 2001, vol. 27.

[19] B. D. O. Anderson and J. B. Moore, *Optimal filtering*, T. Kailath, Ed. Prentice-Hall, Inc., 1979.

[20] M. Morari and E. Zafiriou, *Robust Process Control*. Prentice Hall, Englewood Cliffs, 1989.